

CSS_J154915.7+375506: A low-mass-ratio marginal contact binary system with a hierarchical third body

Jin-Feng Wu,¹²³★ Li-Ying Zhu,¹²³† Azizbek MATEKOV,¹²⁴ Lin-jia Li,¹³ Shuhrat EHGAMBERDIEV,⁴⁵ Ildar ASFANDIYAROV,⁴ Jiang-Jiao Wang,¹²³ Jia Zhang¹³ and Fang-Bin Meng¹²³

¹Yunnan Observatories, Chinese Academy of Sciences (CAS), Kunming 650216, China

²University of Chinese Academy of Sciences, No.1 Yanqihu East Rd, Huairou District, 101408, Beijing, People's Republic of China

³Key Laboratory of the Structure and Evolution of Celestial Objects, Chinese Academy of Sciences, 650216, Kunming, People's Republic of China

⁴Ulugh Beg Astronomical Institute of the Uzbekistan Academy of Science, Astronomicheskaya 33, Tashkent, 100052, Uzbekistan

⁵National University of Uzbekistan, 4 University str, Tashkent, 100174, Uzbekistan

Last updated 2020 June 10; in original form 2013 September 5

ABSTRACT

We presented the multi-filter light curves of CSS_J154915.7+375506 inaugurally, which were observed by the 1.5 m AZT-22 telescope at Maidanak Astronomical Observatory. A low-resolution spectrum obtained by LAMOST reveals it is an A-type close binary. By analyzing the BVRI total-eclipse light curves, we are able to derive a reliable photometric solution for this system, which indicates that CSS_J154915.7+375506 is an extremely low-mass-ratio ($q=0.138$) marginal contact binary system. The location in the HR diagram shows that its secondary component with a much smaller mass is the more evolved one, indicating the mass ratio reversal occurred. The present secondary component had transferred a significant amount of mass to the present primary one. By the combination of a total of 20 times of minimum, we investigated its O-C curve. A periodic oscillation and a possible period decrease have been detected. As the period decreases, the system will evolve towards the contact phase. This makes CSS_J154915.7+375506 a valuable case to study the formation scenario of contact binaries through mass reversal. The periodic oscillation suggested a third body with a minimal mass of $0.91 M_{\odot}$, which is larger than that of the less massive component in the central binary. This implies that the secondary body was not replaced by the third body during early stellar interactions, indicating that it is a fossil system and retains its original dynamical information.

Key words: binaries:close – binaries:eclipsing – stars:evolution – stars:individual(CSS_J154915.7+375506)

1 INTRODUCTION

Eclipsing binary systems exhibiting EB-type light variations, particularly those of short periods, offer captivating insights into the evolutionary transformations experienced by close binary systems. Near-contact binaries (NCBs), an important subclass of close binaries which lie in a key evolutionary stage (Zhu & Qian 2006), were defined by (Shaw et al. 1994). Considering the geometric structure of NCBs, it can be divided into 4 subclasses: SD1 type or SD2 type, semi-detached binaries with star1 or star2 filling its critical Roche lobe; D type, detached binary with components very close to their critical Roche lobe; and C type, marginal contact binary, both components filling their critical Roche lobe with large temperature differences (Zhu & Qian 2009). The marginal contact system is considered a special type of NCB in testing the Thermal relaxation oscillation (TRO) theory (Lucy 1976a; Lucy & Wilson 1979; Flannery 1976). On the basis of TRO theory, the long-term instability of thermal equilibrium in contact configurations results in the status of marginal contact, together the semi-detached constitute two phases of periodic thermal relaxation oscillation.

NCBs which lie in these two phases that sustain such a short time compared to the lifetime of the binary, are rare. So, despite decades of comprehensive research, the properties and evolution on marginal contact binaries still remain blurred. A recently formed contact binary will undergo thermal evolution towards a state of marginal contact, and if the contact is subsequently disrupted, the system will revert back into contact (Lucy 1976b). This implies that a marginal contact binary could represent a pre-contact binary system. The transitional nature of marginal contact binaries is a crucial evolutionary stage that has the potential to enhance our understanding of the evolutionary process of NCBs. Building on this, K. Stepień and M. Kiraga's evolutionary model (Stepień & Kiraga 2013) suggests that contact binaries may have experienced mass ratio reversal in the past. Based on the discussion of marginal contact binaries above, we will now introduce our upcoming research, which will delve into a specific marginal contact binary.

The short-period near contact binary CSS_J154915.7+375506 ($\alpha_{J2000} = 15^h 49^m 15^s.7, \delta_{J2000} = +37^{\circ} 55' 06''$, also named UCAC4 640-050794, CRTS J154915.7+375506, ATO J237.3156+37.9183) was found as an EW-type eclipsing binary with a period of 0.377998 days and mean $V_{mag} = 13.88 mag$ in the

★ E-mail: wujinfeng@ynao.ac.cn

† E-mail: zhuly@ynao.ac.cn

Table 1. The coordinates of CSS_J154915.7+375506, the comparison star and the check star.

| Stars | α_{2000} | δ_{2000} |
|----------------------|---|-----------------|
| CSS_J154915.7+375506 | 15 ^h 49 ^m 15 ^s .76 | +37°55′06″.01 |
| The comparison | 15 ^h 49 ^m 08 ^s .88 | +37°50′21″.19 |
| The check | 15 ^h 49 ^m 09 ^s .79 | +37°55′18″.64 |

Catalina Surveys Data Release-1 (CSDR1)(Drake et al. 2014). In 2017, it was included in the Czech Variable Star Catalogue(Skarka et al. 2017), whereafter it was observed by the Catalina Real-Time Transient Survey (CRTS)(Marsh et al. 2017) with a light curve displayed and identified as an EB-type binary. This target was observed by the AZT-22 telescope of the Maidanak Astronomical Observatory (MAO), and multicolor light curves were obtained. It was also observed by the Large sky Area Multi-Object fiber Spectroscopic Telescope ((Luo et al. 2012; Zhao et al. 2012)) in 14th, April 2017, and the atmospheric parameters of the system were determined. The primary effective temperature $T_1 = 6929.5 K$ was adopted in our study. Our results show that this target is a marginal contact binary system with an extremely low mass ratio of 0.138, which means the mass ratio reversal occurred. The O-C curve analysis demonstrates that a third body may exist.

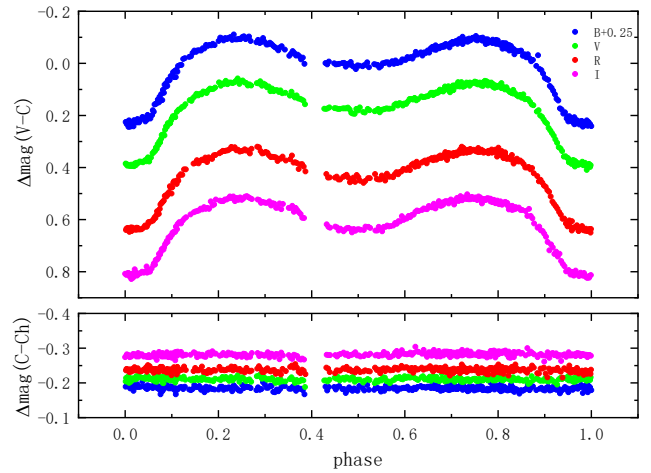
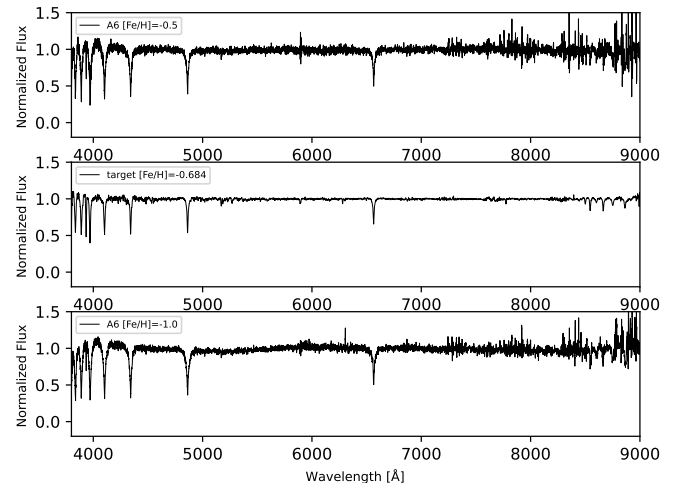
2 PHOTOMETRIC AND SPECTRAL OBSERVATIONS

2.1 Photometric Data

New photometric observations of the variable star CSS_J154915.7+375506 were carried out by the 1.5-m telescope AZT-22 on February 23, April 23, and June 23, 2023, at the Maidanak Astronomical Observatory (MAO) of the Ulugh Beg Astronomical Institute of the Uzbekistan Academy of Science (Ehgamberdiev 2018). The optical system of the AZT-22 telescope is Ritchey-Chretien, and the focal length is 11560 mm (Artamonov 1998). The Andor iKon-XL (XL-EA07-DS) (4096(H) × 4108(V)) CCD camera was used as the receiver. The read-out noise and amplification coefficients of the CCD camera are 6.5ADUs and 1.55 e-, the effective field of view is 18.1′ × 18.1′ arcmin, and the pixel scale is 0.268′ arcsec per pixel. In combination with the CCD detector, these provided a photometric system close to the standard Bessell UBVR system (Im et al. 2010). Image acquisition was done with MaxIm DL 6 version. The observations were using the BVRI filters of the Bessell photometric system at 30, 20, 10 and 10 second exposure times, respectively. Figure 1 shows the EB multicolor light curves, and the standard deviation of the comparison minus the check are 0.00683, 0.00524, 0.00622 and 0.00582 for B, V, R and I, respectively. The coordinates of the comparison and check stars are listed in Table 1. In the light curves, the difference between the primary minimum and the secondary is close to 0.2 mag, with the flat primary minimum, this system should be a total eclipse binary.

2.2 LAMOST Spectrum

LAMOST is a reflective Schmidt telescope with a 4-meter aperture and a 5-degree field of view, which is located at the Xinglong Observatory in Hebei, China. With 4000 fibers placed on the focal plane, LAMOST can obtain 4000 spectra simultaneously. Meanwhile, stellar atmospheric parameters can be obtained automatically by the LAMOST stellar parameter pipeline (LASP) (Wu et al. 2011, 2014; Luo et al. 2015). The low-resolution spectrum of LAMOST

**Figure 1.** The light curves of CSS_J154915.7+375506 in the Bessell B, V, R and I bands were observed by the 1.5 m AZT-22 telescope. The magnitude difference of the comparison star minus the check star (C-Ch) is shown in the bottom panel.**Figure 2.** Spectra figures. Upper panel: A normalized A6 spectral template with $[Fe/H] = -0.5$. Middle panel: the normalized spectrum of CSS_J154915.7+375506. Lower panel: A normalized A6 spectral template with $[Fe/H] = -1.0$.

is $R 1800$ and the wavelength range is 3700-9100Å. We found one low-resolution spectrum from the LAMOST DATA RELEASE 9 and obtained the atmospheric parameters as spectral type: A6, surface effective temperature: 6929.51 K, surface gravity: 4.259 dex and the metallicity: -0.684. The normalized spectrum is shown in Figure 2, in which located in the upper panel and lower panel are A6 type spectral template(Kesseli et al. 2017) for comparison.

3 LIGHT CURVE ANALYSIS

The Wilson-Devinney(Wilson & Devinney 1971; Wilson 1990; Wilson 2012; Wilson & Hamme 2013) code was applied to analyze the multicolor light curves. The surface effective temperature of the primary component was set to $T_1 = 6930 K$ according to the stellar

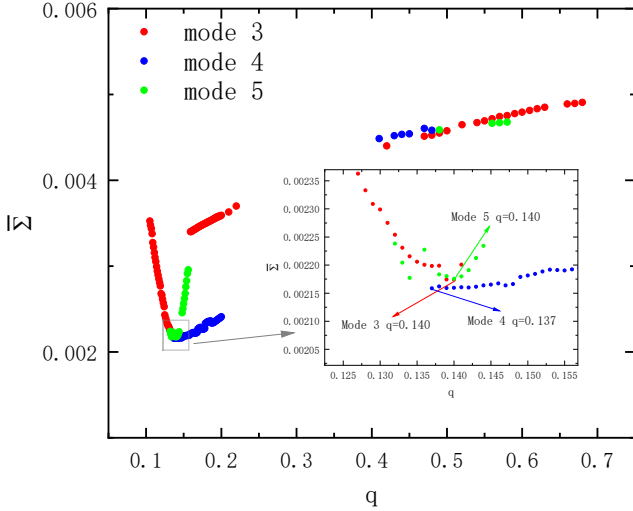


Figure 3. The relationship between q and the mean weighted residuals $\bar{\Sigma}$ for Mode 4 and Mode 5.

atmospheric parameters of LAMOST. The gravity-darkening coefficients $g_1 = 0.32$ and $g_2 = 0.32$ (Lucy 1967), the bolometric albedo $A_1 = 0.5$ and $A_2 = 0.5$ (Rucinski 1969) were adopted. We tried to adopt mode 2 (detached binary), mode 3 (overcontact binary), mode 4 (semidetached binary with star 1 nearly filling its Roche lobe) and mode 5 (semidetached binary with star 2 nearly filling its Roche lobe) to fit the light curves but mode 2 failed to converge. We used the q -search method to derive initial mass ratio. For mode 3, 4 and 5, convergent solutions were obtained when the mass ratio was fixed as a series of values from 0.1 to 1 with a step of 0.001. The minimum values of Σ were achieved at similar q values: 0.140, 0.137 and 0.140, respectively, which indicates the reliability of the mass ratio. The q -search diagram is shown in Figure 3. After that, we set the q with the value 0.137 and rerun to run the WD code for the three modes. The other adjustable parameters of mode 3 are the orbital inclination, i , the mean surface temperature of the secondary component, T_2 , the dimensionless potential of the primary, Ω_1 (with $\Omega_2 = \Omega_1$), the band-pass luminosity of the primary, L_1 , and the third light, L_3 . For mode 4, the only difference with mode 3 is the adjustable dimensionless surface potential is of the secondary, Ω_2 . As for mode 5, the adjustable parameters are the same as that of mode 3 (with $\Omega_1 \neq \Omega_2$). All the convergent solutions are listed in Table 2. The Σ can be noticed in the last row of the table, and no large difference exists; as an example, the fitted light curves of mode 3 with and without L_3 are shown in Figure 4. It can be seen from Figure 4 that the fits with L_3 look almost identical to the fits without L_3 but smaller residuals can be noticed from the Table 2. So CSS_J154915.7+375506 may be a marginal contact binary with an extremely low mass ratio, with the low contribution of third light, a faint third companion could exist.

4 ORBITAL PERIOD INVESTIGATION

Orbital period variations are common in binary systems which are usually caused by angular momentum loss, mass transfer, third body or magnetic activity. We used the O-C method to analyze the orbital period variation of this system. To obtain more light minimum times, we tried to search for more photometric data from the sky

survey project and public databases. We collected data from All-Sky Automated Survey for Supernovae (ASAS-SN) (Shappee et al. 2014; Christy et al. 2023) database, Catalina Real-Time Transient Survey (CRTS) (Drake et al. 2009) database, The Zwicky Transient Facility (ZTF) (Bellm et al. 2018) and Transiting Exoplanet Survey Satellite (TESS) (Ricker et al. 2010) which provided Full Frame Images (FFI) for three sectors with an exposure time of the 1800s, 600s and 600s. We converted data with more than one cycle into a phase (Shi et al. 2021; Li et al. 2022) to get the minima by using parabola fitting. Some data of the ASAS-SN is shown in the left panel of Figure 5 and the right panel shows the light curve converted to one phase. Finally, we obtained 2 times of minimum from ASAS-SN, 2 times of minimum from CRTS, 5 times of minimum from ZTF and 10 times of minimum from TESS, plus the 1 fitted from AZT-22 data, 20 in total. The times of light minima are listed in the first column of the Table 3. The $O - C$ values were calculated with the following linear ephemeris formula:

$$\text{Min.}I(HJD) = 2457208.72017397 + 0^d.377998 \times E \quad (1)$$

In which the HJD_0 and period value was obtained from The International Variable Star Index (VSX)¹. In O-C curves, it is clear that a periodic oscillation exists which may be caused by the light time travel effect (LTTE) of a third body (Liao & Qian 2010). We use the following general equation to fit the O-C diagram (Irwin 1952):

$$\begin{aligned} O - C &= \Delta T_0 + \Delta P_0 E + \frac{\beta}{2} E^2 \\ &+ A \left[(1 - e_3^2) \frac{\sin(v + \omega)}{1 + e_3 \cos v} + e \sin \omega \right] \\ &= \Delta T_0 + \Delta P_0 E + \frac{\beta}{2} E^2 \\ &+ A \left[\sqrt{1 - e_3^2} \sin E^* \cos \omega + \cos E^* \sin \omega \right] \end{aligned} \quad (2)$$

The Kepler equation is as follows:

$$M = E^* - e_3 \sin E^* = \frac{2\pi}{P_3} (t - T_3) \quad (3)$$

the meaning of each parameter is described very clearly in the paper (Liao et al. 2021). The corresponding results of Equations 2 and 3 are displayed in Table 4. Based on the existence of the periodic oscillation, we assumed a circular orbit ($e_3 = 0$), i.e. (1) Case A, the linear term plus cyclical variation ($\beta = 0$) and (2) Case B, the quadratic term plus cyclical variation ($\beta \neq 0$). In addition, we considered an eccentric orbit ($e_3 \neq 0$) with a linear term, i.e. (3) Case C, the linear term plus eccentric orbit ($\beta = 0$). By using Equation 2 and 3 to fit the O-C curve, the results of the three cases are listed in Table 4. The fitted O-C curve and the residuals for different cases are shown in Figure 6. For Case A, the amplitude and period of the cyclical variation are $A = 0.0142(\pm 0.0006)$ days and $P_3 = 12.48(\pm 0.25)$ yr. For Case B, the amplitude and period of the cyclical variation are $0.0145(\pm 0.0010)$ days and $P_3 = 14.89(\pm 0.96)$ yr with a long-term period decrease at a rate: $\beta = -3.25 \times 10^{-10}$ d cycle⁻¹, i.e. $-3.14(\pm 0.89) \times 10^{-7}$ days yr⁻¹. We can see different possible O-C curve variations correspond to different cases, but a common periodic oscillation may imply an existence of a third body, so further investigations are necessary. As for the Case C, the eccentricity of the third body is $e_3 = 0.40(\pm 0.15)$, the amplitude and period of the cyclical variation are $A = 0.0175(\pm 0.0029)$ days and $P_3 = 12.37(\pm 0.11)$ yr, respectively.

¹ <https://www.aavso.org/vsx/>

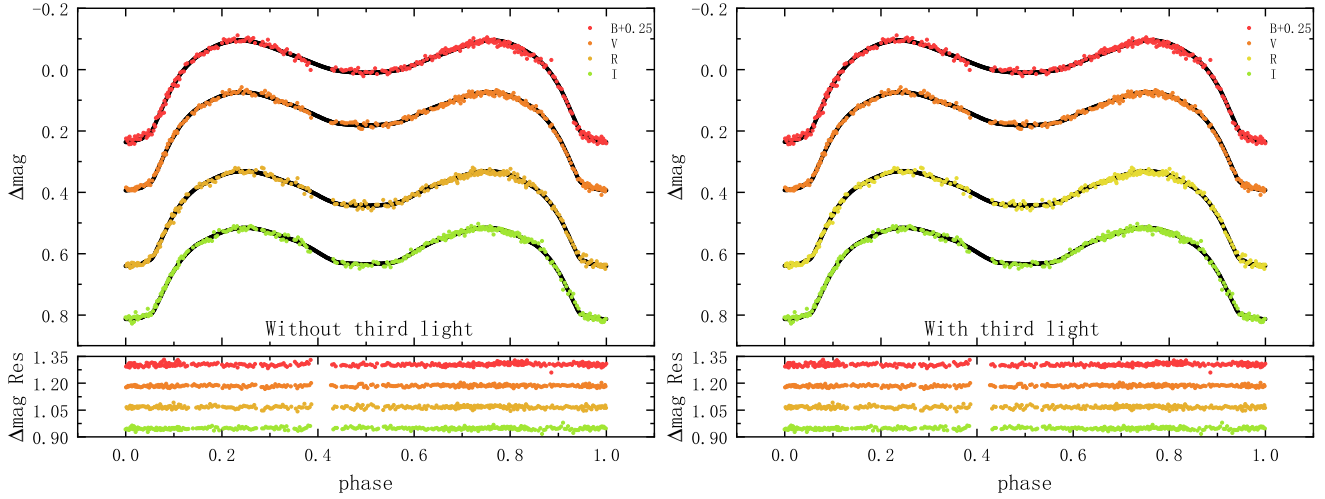


Figure 4. Multiband observational and theoretical light curves of CSS_J154915.7+375506 in B, V, R and I bands from MAO AZT-22. The left-upper panel is the light curve without L_3 while the right-upper panel is the light curve with L_3 . In the bottom panel, the residuals of the observations minus the theoretical light curves are shown. The residuals are vertical moved to display well.

Table 2. Photometric solutions of CSS_J154915.7+375506 obtained by using the W-D code. The units of most parameters are dimensionless, except those already mentioned.

| Parameters | Mode 3 | | Mode 4 | | Mode 5 | |
|---------------------------|------------------|---|---------------|--------------|---------------|--------------|
| | Without L_3 | With L_3 | Without L_3 | With L_3 | Without L_3 | With L_3 |
| $g_1 = g_2$ | 0.32 | 0.32 | 0.32 | 0.32 | 0.32 | 0.32 |
| $A_1 = A_2$ | 0.5 | 0.5 | 0.5 | 0.5 | 0.5 | 0.5 |
| $q (M_2/M_1)$ | 0.13875(55) | 0.13824(91) | 0.13828(46) | 0.13828(89) | 0.13729(28) | 0.13696(61) |
| $i (^\circ)$ | 86.153(97) | 86.151(97) | 85.796(95) | 85.796(98) | 87.17(12) | 87.02(11) |
| $T_1 (K)$ | 6930 | 6930 | 6930 | 6930 | 6930 | 6930 |
| $T_2 (K)$ | 4209(33) | 4210(33) | 4184(30) | 4184(31) | 4225(30) | 4223(32) |
| Ω_1 | 2.0720(22) | 2.0706(24) | 2.07088 | 2.07088 | 2.07093(36) | 2.07007(43) |
| Ω_2 | 2.0720(22) | 2.0706(24) | 2.0714(21) | 2.0714(21) | 2.06814 | 2.06722 |
| $L_1/(L_1 + L_2)_B$ | 0.9951413(26) | 0.995146(35) | 0.9954392(21) | 0.995439(39) | 0.9949932(25) | 0.995026(22) |
| $L_1/(L_1 + L_2)_V$ | 0.9892739(82) | 0.989289(86) | 0.9898197(72) | 0.989820(97) | 0.9890236(81) | 0.989085(59) |
| $L_1/(L_1 + L_2)_R$ | 0.982783(16) | 0.98281(15) | 0.983541(15) | 0.98354(17) | 0.982461(16) | 0.98255(11) |
| $L_1/(L_1 + L_2)_I$ | 0.974829(26) | 0.97488(24) | 0.975723(25) | 0.97572(27) | 0.974491(26) | 0.97460(18) |
| $L_3/(L_1 + L_2 + L_3)_B$ | – | 0.0131(65) | – | 0.0126(75) | – | 0.0113(42) |
| $L_3/(L_1 + L_2 + L_3)_V$ | – | 0.010711(86) | – | 0.0018(86) | – | 0.0003(51) |
| $L_3/(L_1 + L_2 + L_3)_R$ | – | 0.00048(838) | – | 0.0011(93) | – | 0.0000(61) |
| $L_3/(L_1 + L_2 + L_3)_I$ | – | $9.4 \times 10^{-5} (9.2 \times 10^{-3})$ | – | 0.0019(102) | – | 0.0000(70) |
| $r_1 (pole)$ | 0.51311(44) | 0.51329(45) | 0.51338(23) | 0.51328(44) | 0.51316(10) | 0.51328(16) |
| $r_1 (side)$ | 0.56504(64) | 0.5653(065) | 0.56543(32) | 0.56529(62) | 0.56505(16) | 0.56521(27) |
| $r_1 (back)$ | 0.58524(67) | 0.58551(67) | 0.58566(3) | 0.58552(57) | 0.58504(21) | 0.58518(40) |
| $r_2 (pole)$ | 0.2175(21) | 0.2176(3) | 0.2172(18) | 0.2175(27) | 0.21698(13) | 0.21684(28) |
| $r_2 (side)$ | 0.2092(18) | 0.2093(25) | 0.209(16) | 0.2092(23) | 0.20869(13) | 0.20856(27) |
| $r_2 (back)$ | 0.2492(40) | 0.2495(58) | 0.2488(35) | 0.2492(53) | 0.24868(14) | 0.24853(29) |
| <i>fill – out factor</i> | 0.00231(0.02415) | 0.00228(0.026452) | – | – | – | – |
| Σ | 0.00204 | 0.00169 | 0.00203 | 0.00169 | 0.00203 | 0.00170 |

5 DISCUSSION AND CONCLUSION

5.1 Absolute parameters

The orbital period analysis and multicolor CCD photometric solutions of CSS_J154915.7+375506 are presented for the first time. With the newly observed multicolor light curves, good photometric solutions on mode 3, mode 4 and mode 5 were obtained by using W-D code. Although the radial velocity curve is missing, it is a total eclipse binary system, and all solutions show similar mass ratios, so the results are reliable. The solutions are shown to us in Table 2 that

all the convergent solutions are with very close parameter values and similar residuals, and all solutions with L_3 have smaller residuals, so we will take the average values of the results with L_3 for the following discussions.

Combined with the photometric solutions and parallax, the absolute parameters can be estimated by the method described by (Li et al. 2021) and (Xu et al. 2022). The parallax ϖ was given by Gaia Dr3 as 0.6934 mas, so the distance was estimated as about 1442 pc, which was calculated by the following formula:

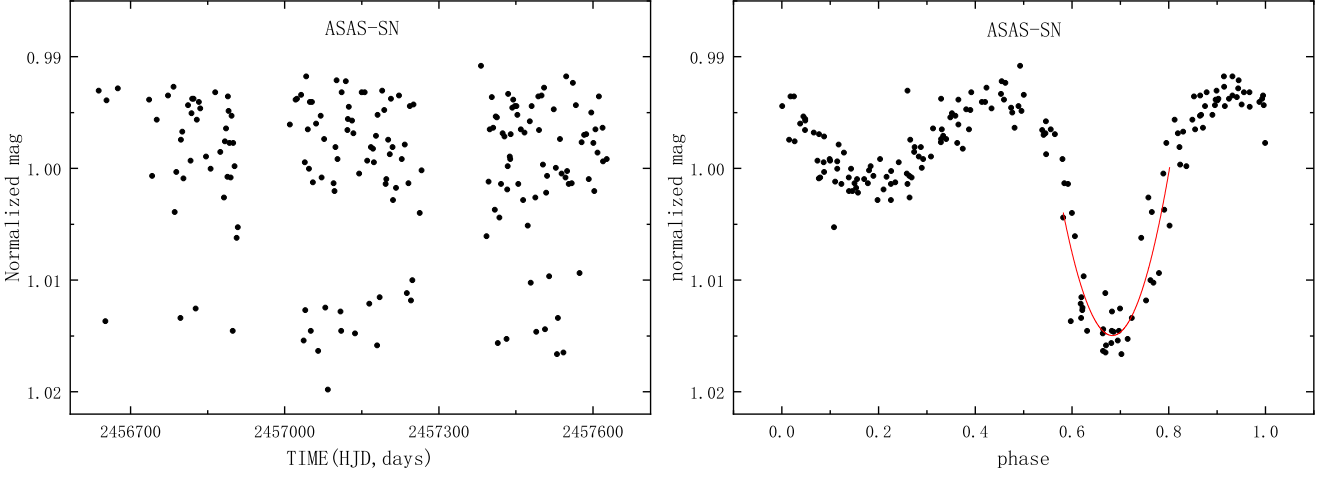


Figure 5. Left panel: ASAS-SN photometric data in V band. Right panel: Light curve converted to one phase and fitted the light minima phase with a parabola function.

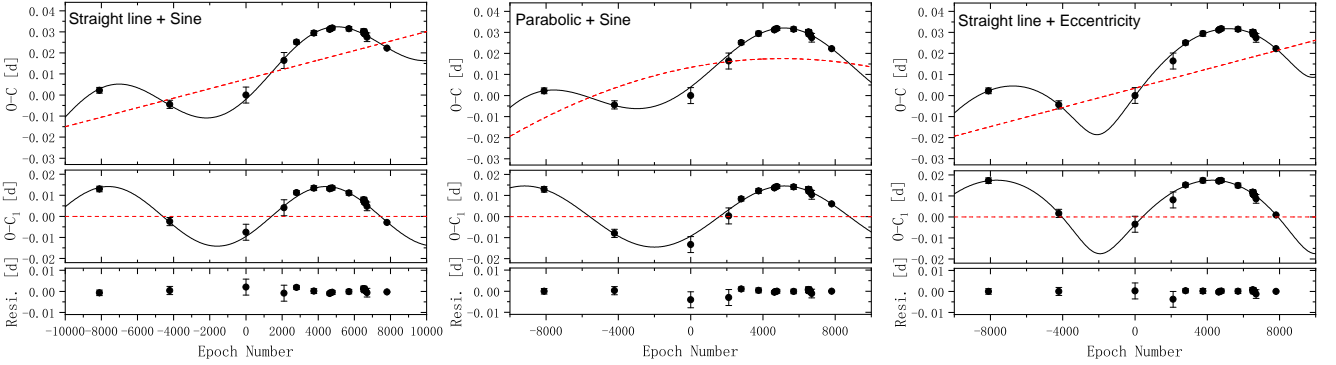


Figure 6. The O-C curve from the linear ephemeris of equation (1) are shown in the upper panel, the middle panel shows the fitted results of linear term plus cyclical variation, quadratic term plus cyclical variation and linear term plus eccentric orbit and the bottom panel shows the residuals of O-C curve removed all variations.

$$(m - M)_v = 10 - 5 \lg \varpi + A_v \quad (4)$$

where the extinction A_v is 0.035 mag (obtained from the NASA/IPAC Extragalactic Database²), and the apparent magnitude m_v is 13.776 mag, the maximum brightness in the V band from ASAS-SN data (Shappee et al. 2014; Christy et al. 2023). Then with the bolometric correction $BC_v = -0.07$ mag (Worthey & Lee 2011), we can obtain its bolometric absolute magnitude M_v with this equation:

$$M_{bol} = M_v + BC_v \quad (5)$$

hence, the total luminosity L_t of the binary system is derived by:

$$L_T = L_1 + L_2 = 10^{(M_{bol} - 4.74) / -2.5} \quad (6)$$

And with the Stefan Boltzmann's law, we have:

$$L_t / L_\odot = (ar_1)^2 \times \left(\frac{T_1}{T_\odot}\right)^4 + (ar_2)^2 \times \left(\frac{T_2}{T_\odot}\right)^4 \quad (7)$$

where T_\odot represents the effective temperature of the sun, with a value of 5772 K. r_1 and r_2 represent the relative radii of the star 1 and star 2, respectively, which can be obtained from the photometric solutions, just like $r_i = (r_{ipole} * r_{iside} * r_{iback})^{1/3}$. The semi-major axis a is obtained as about $2.92 R_\odot$. Combined with the mass ratio and the Kepler's third law,

$$\frac{a^3}{p^2} = 74.5(M_1 + M_2), \quad (8)$$

$$q = \frac{M_2}{M_1} \quad (9)$$

the mass of the primary component M_1 and the mass of the secondary component M_2 were calculated about $2.05 M_\odot$ and $0.283 M_\odot$, respectively. All the estimated absolute parameters are tabulated in Table 5.

5.2 Orbital period variations

In the present paper, the orbital period changes are studied for the first time by analyzing a total of 20 times of minima with time span

² https://ned.ipac.caltech.edu/extinction_calculator

Table 3. The light minima of CSS_J154915.7+375506.

| Eclipse timings (HJD) | Error (\pm d) | E | O-C (d) | Reference |
|-----------------------|------------------|-------|-------------|-----------|
| 2457208.72 | 0.001432612 | 0 | 0.00000000 | ASAS-SN |
| 2458005.934 | 0.001436392 | 2109 | 0.01637465 | ASAS-SN |
| 2454143.537 | 0.000506517 | -8109 | 0.00223421 | CRTS |
| 2455615.454 | 0.000971455 | -4215 | -0.00444866 | CRTS |
| 2458269.408 | 0.000374218 | 2806 | 0.02509633 | ZTF |
| 2458630.022 | 0.000442258 | 3760 | 0.02942852 | ZTF |
| 2459015.204 | 0.000351538 | 4779 | 0.03178869 | ZTF |
| 2459363.34 | 0.000408238 | 5700 | 0.03150496 | ZTF |
| 2459743.98 | 0.000782456 | 6707 | 0.0274099 | ZTF |
| 2460161.285 | 0.0002675 | 7811 | 0.02224803 | AZT-22 |
| 2458962.284 | 0.000287278 | 4639 | 0.03109575 | TESS s24 |
| 2458975.892 | 0.000238139 | 4675 | 0.03143317 | TESS s24 |
| 2459669.139 | 0.000487617 | 6509 | 0.03005764 | TESS s50 |
| 2459675.565 | 0.000449818 | 6526 | 0.03010509 | TESS s50 |
| 2459682.747 | 0.000540537 | 6545 | 0.0295658 | TESS s50 |
| 2459688.795 | 0.000389338 | 6561 | 0.0295849 | TESS s50 |
| 2459695.976 | 0.000287278 | 6580 | 0.02904642 | TESS s51 |
| 2459702.024 | 0.000241919 | 6596 | 0.02900456 | TESS s51 |
| 2459708.828 | 0.000351538 | 6614 | 0.02884077 | TESS s51 |
| 2459714.876 | 0.000268379 | 6630 | 0.02880401 | TESS s51 |

of 16 years. In Case B, a long-term period decrease and periodic oscillation are revealed with $\beta = -3.14(\pm 0.89) \times 10^{-7} \text{ days yr}^{-1}$. According to the period variation equation:

$$\frac{\dot{P}}{P} = -3\left(\frac{\dot{M}_1}{M_1} + \frac{\dot{M}_2}{M_2}\right), \quad (10)$$

we can get the rate of mass transfer from the primary to the secondary is $\dot{M}_1 = -9.1(\pm 2.8) \times 10^{-8} M_\odot \text{ yr}^{-1}$. Without more long-term observations, we cannot determine whether the period decrease exists or not. In general, all cases of O-C curve analysis show evidences of the periodic oscillation. Considering that the target is an A-type marginal contact binary and photometric solutions with third lights from symmetrical light curves were obtained, the oscillations are mostly caused by the LTTE of a third body. In order to do further study on the period variation, we use the following formula to estimate the possible parameters of the third body:

$$f(m) = \frac{(M_3 \sin i_3)^3}{(M_1 + M_2 + M_3)^2} = \frac{4\pi^2}{GP_3^2} \times (a_{12} \sin i_3)^3, \quad (11)$$

the mass function of this system is $f(m) = 0.10(\pm 0.01) M_\odot$ for Case A, $f(m) = 0.07(\pm 0.02) M_\odot$ for Case B and $f(m) = 0.18(\pm 0.09) M_\odot$ for Case C. By assuming the orbital inclination $i_3 = 90^\circ$, we can estimate the minimum mass of the third body are $M_3 = 1.02(\pm 0.05) M_\odot$, $M_3 = 0.91(\pm 0.06) M_\odot$ and $M_3 = 1.36(\pm 0.19) M_\odot$ respectively. However, considering the extremely low contribution of the third light, this third body may be not in its main-sequence stage, perhaps an unseen compact object. Some statistics indicate that third bodies are common in contact binaries (Tokovinin et al. 2006; Pribulla & Rucinski 2006; D'Angelo et al. 2006; Rucinski et al. 2007), and the existence of a third body may play an important role in the binary's evolution. Core fragmentation is thought to be the way to form binary system (Boss 1986; Bate et al. 1995). However, binaries yielded by this mechanism correspond to initial separations range of 10 to 1000 au. One way of

Table 4. Orbital parameters of the third body in CSS_J154915.7+375506.

| Parameter | Value | Unit |
|---|-----------------------------------|-----------------------|
| Case A: linear term plus cyclical variation ($\beta = 0$) | | |
| Revised epoch, T_0 | 2457208.7277(± 0.0007) | HJD |
| Revised period, P_0 | 0.37800020(± 0.00000010) | days |
| Eccentricity, e_3 | 0 (assumed) | – |
| Long-term change of the orbital period, β | 0 (assumed) | d cycle ⁻¹ |
| Orbital period, P_3 | 12.48(± 0.25) | yr |
| Amplitude, A | 0.0142(± 0.0006) | days |
| Projected semi-major axis, $a_{12} \sin(i_3)$ | 2.45(± 0.10) | au |
| Mass function, $f(m)$ | 0.10(± 0.01) | M_\odot |
| Mass, M_{3min} | 1.02(± 0.05) | M_\odot |
| Sum of the squares of the residuals, Σ | 1.66×10^{-5} | – |
| Case B: quadratic term plus cyclical variation ($\beta \neq 0$) | | |
| Revised epoch, T_0 | 2457208.7335(± 0.0017) | HJD |
| Revised period, P_0 | 0.37798160(± 0.00000030) | days |
| Eccentricity, e_3 | 0 (assumed) | – |
| Long-term change of the orbital period, β | $-3.25(\pm 0.89) \times 10^{-10}$ | d cycle ⁻¹ |
| Orbital period, P_3 | 14.89(± 0.96) | yr |
| Amplitude, A | 0.0145(± 0.0010) | days |
| Projected semi-major axis, $a_{12} \sin(i_3)$ | 2.51(± 0.17) | au |
| Mass function, $f(m)$ | 0.07(± 0.02) | M_\odot |
| Mass, M_{3min} | 0.91(± 0.06) | M_\odot |
| Sum of the squares of the residuals, Σ | 2.98×10^{-5} | – |
| Case C: linear term plus eccentric orbit ($\beta = 0$) | | |
| Revised epoch, T_0 | 2457208.7237(± 0.0030) | HJD |
| Revised period, P_0 | 0.37800028(± 0.00000005) | days |
| Eccentricity, e_3 | 0.40(± 0.15) | – |
| Long-term change of the orbital period, β | 0 (assumed) | d cycle ⁻¹ |
| Orbital period, P_3 | 12.37(± 0.11) | yr |
| Amplitude, A | 0.0175(± 0.0029) | days |
| Longitude of the periastron passage, ω_3 | 260.02(± 8.85) | degree |
| Time of periastron passage, T_3 | 2456409.0183(± 120.5700) | days |
| Projected semi-major axis, $a_{12} \sin(i_3)$ | 3.03(± 0.50) | au |
| Mass function, $f(m)$ | 0.18(± 0.09) | M_\odot |
| Mass, M_{3min} | 1.36(± 0.19) | M_\odot |
| Sum of the squares of the residuals, Σ | 1.73×10^{-5} | – |

Table 5. Estimated absolute parameters of CSS_J154915.7+375506

| Parameters | Value | Parameters | Value |
|-----------------|---------------|------------|--------------|
| ϖ (mas) | 0.6934(0.014) | A_v | 0.035 |
| m_V | 13.776(0.023) | M_v | 2.95(0.05) |
| M_{bol} | 2.88(0.05) | BC_V | -0.07 |
| M_1 | 2.05(0.15) | M_2 | 0.283(0.02) |
| R_1 | 1.62(0.04) | R_2 | 0.656(0.016) |
| L_1 | 5.43(0.27) | L_2 | 0.121(0.006) |
| semi major axis | 2.92(0.07) | | |

forming closer binaries is dynamical interactions with other nearby stars (Bate et al. 2002). Dynamical interactions often result in the replacement of the lower-mass binary component with a higher-mass third body. Consequently, the original system undergoes a process where the lower-mass component is ejected to a wider orbit, forming a hierarchical triple system. Through the passage of time, these processes have a tendency to give rise to binary systems featuring closely spaced components and almost equivalent masses (Bate et al. 2002; Gullikson & Dodson-Robinson 2013). Based on our system, the mass of the third body is greater than that of the secondary component, indicating that CSS_J154915.7+375506 is the original one and was not replaced by the third body. Therefore, the third carried some dynamical characteristics during binary star formation.

5.3 Discussion

Hertzsprung-Russell diagram with $[Fe/H] = -0.75$ was displayed in Figure 7. The primary and secondary of this system are plotted in this figure. Besides, we plotted 700 contact binaries (Latković et al. 2021) and selected spectral A type contact binaries by setting the primary temperature range $6900 K < T_1 < 9000 K$. From this diagram, normal contact binaries' primary components are usually more evolved, while the secondary is not. As for A type contact binaries, most of the primaries are evolved to near the TAMS (terminal-age main-sequence), and the secondaries just went through the ZAMS (zero-age main-sequence) (Dotter 2016; Choi et al. 2016). CSS_J154915.7+375506 is different, the primary component is in main-sequence near the TAMS, while the secondary seems to just deviate from the TAMS. Under this situation: the extremely low mass ratio of 0.138 with the mass of the secondary of $0.283 M_{\odot}$, which is much less than the primary component. The secondary should not have evolved so quickly on its own (Clayton 1983; Paczyński 1971), so it must be caused by the interaction between the two components.

Now let's consider the aspect of mutual influence between the binary components. On the one hand, the secondary star has a much smaller mass than the primary star, but it is more evolved, indicating that the secondary star was once the primary star. It evolved faster and transferred a large amount of mass to the current primary star (Crawford 1955). Its characteristic of marginal contact indicates that this system has just experienced a mass ratio reversal and is evolving towards the next stage.

On the other hand, the current photometric solutions indicate that the mass of the secondary star is $0.283 M_{\odot}$, but the temperature is higher than 4000 K. This suggests that the secondary star, after evolving and expanding, has shed its outer material and exposed part of its core, which is why its current temperature is relatively high. According to the O-C curve analysis, if the long-term period decreasing really exists, the system will evolve to be a contact binary.

5.4 Conclusion

In conclusion, the distinct characteristics of CSS_J154915.7+375506, including its exceptionally low mass ratio and the evolutionary status of its secondary component, together with its high temperature relative to its mass, suggest that the system has undergone significant mass transfer, likely experienced a mass ratio reversal event. Furthermore, considering the evidence from current photometric solutions and the potential for long-term period decrease based on O-C curve analysis, the system may evolve towards becoming a contact binary. Therefore, CSS_J154915.7+375506 serves as an intriguing subject for investi-

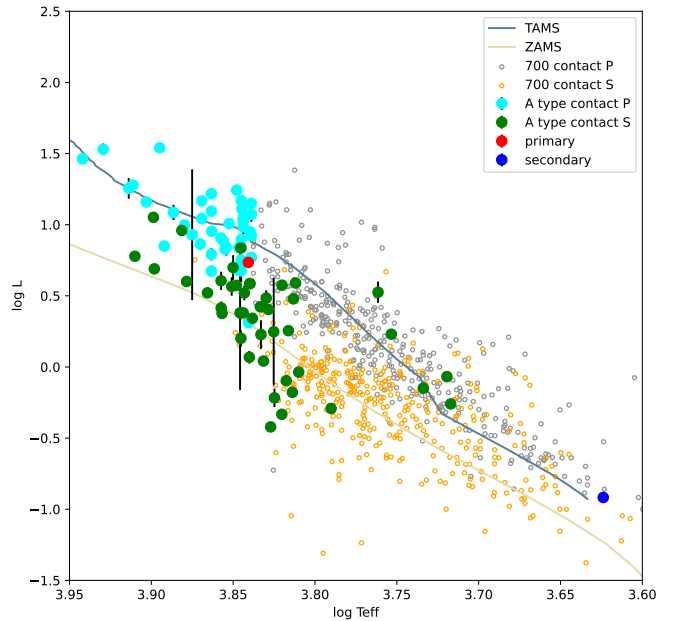


Figure 7. The positions of the primary and secondary component of CSS_J154915.7+375506 in the H-R diagram.

gating the formation processes and evolutionary pathways of binary systems.

6 DATA AVAILABILITY

The data underlying this article will be uploaded to the VizieR data base (CDS).

ACKNOWLEDGEMENTS

This work is supported by the International Cooperation Projects of the National Key R&D Program (No. 2022YFE0127300), the Science Foundation of Yunnan Province (No. 202401AS070046), the National Natural Science Foundation of China (Nos. 11933008 and 11922306), the Agency of innovative development under the Ministry of higher education, science and innovation of the Republic of Uzbekistan. Project (AL-5921122128): "Investigations and observations of special LAMOST eclipsing binaries based on telescopes in Uzbekistan and China", CAS "Light of West China" Program and Yunnan Revitalization Talent Support Program. The new CCD photometric data were obtained with the Maidanak Astronomical Observatory 1.5 m telescope. This work has made use of data from the All-Sky Automated Survey for Supernovae (ASAS-SN), Catalina Real-Time Transient Survey (CRTS), The Zwicky Transient Facility (ZTF), the Large-Sky-Area Multi-Object Fiber Spectroscopic Telescope (LAMOST), the Transiting Exoplanet Survey Satellite (TESS), and Gaia and the authors thank the teams for providing open data.

REFERENCES

- Artamonov B., 1998, in Symposium-International Astronomical Union. pp 121–122
 Bate M. R., Bonnell I. A., Price N. M., 1995, *MNRAS*, **277**, 362
 Bate M. R., Bonnell I. A., Bromm V., 2002, *MNRAS*, **336**, 705

Bellm E. C., et al., 2018, *Publications of the Astronomical Society of the Pacific*, 131, 018002

Boss A. P., 1986, *ApJS*, 62, 519

Choi J., Dotter A., Conroy C., Cantiello M., Paxton B., Johnson B. D., 2016, *ApJ*, 823, 102

Christy C. T., et al., 2023, *MNRAS*, 519, 5271

Clayton D. D., 1983, *Principles of stellar evolution and nucleosynthesis*. University of Chicago press

Crawford J., 1955, *Astrophysical Journal*, vol. 121, p. 71, 121, 71

D'Angelo C., van Kerkwijk M. H., Rucinski S. M., 2006, *AJ*, 132, 650

Dotter A., 2016, *ApJS*, 222, 8

Drake A. J., et al., 2009, *ApJ*, 696, 870

Drake A. J., et al., 2014, *The Astrophysical Journal Supplement Series*, 213, 9

Ehgamberdiev S., 2018, *Nature Astronomy*, 2, 349

Flannery B. P., 1976, *The Astrophysical Journal*, 205, 217

Gullikson K., Dodson-Robinson S., 2013, *AJ*, 145, 3

Im M.-S., Ko J.-W., Cho Y.-S., Choi C.-S., Jeon Y.-S., Lee I.-D., Ibrahimov M., 2010, *Journal of Korean Astronomical Society*, 43, 75

Irwin J. B., 1952, *The Astrophysical Journal*, 116, 211

Kesseli A. Y., West A. A., Veyette M., Harrison B., Feldman D., Bochanski J. J., 2017, *ApJS*, 230, 16

Latković O., Čeki A., Lazarević S., 2021, *ApJS*, 254, 10

Li K., et al., 2021, *AJ*, 162, 13

Li F. X., Liao W. P., Qian S. B., Fernández Lajús E., Zhang J., Zhao E. G., 2022, *ApJ*, 924, 30

Liao W.-P., Qian S.-B., 2010, *Monthly Notices of the Royal Astronomical Society*, 405, 1930

Liao W., Qian S., Li L., 2021, *Monthly Notices of the Royal Astronomical Society*, 508, 6111

Lucy L. B., 1967, *Z. Astrophys.*, 65, 89

Lucy L. B., 1976a, *ApJ*, 205, 205

Lucy L. B., 1976b, *ApJ*, 205, 208

Lucy L. B., Wilson R. E., 1979, *The Astrophysical Journal*, 231, 502

Luo A. L., et al., 2012, *Research in Astronomy and Astrophysics*, 12, 1243

Luo A.-L., et al., 2015, *Research in Astronomy and Astrophysics*, 15, 1095

Marsh F. M., Prince T. A., Mahabal A. A., Bellm E. C., Drake A. J., Djorgovski S. G., 2017, *MNRAS*, 465, 4678

Paczynski B., 1971, *ARA&A*, 9, 183

Pribulla T., Rucinski S. M., 2006, *AJ*, 131, 2986

Ricker G. R., et al., 2010, in *American Astronomical Society Meeting Abstracts# 215*. pp 450–06

Rucinski S., 1969, *Acta Astronomica*, Vol. 19, p. 245, 19, 245

Rucinski S. M., Pribulla T., van Kerkwijk M. H., 2007, *AJ*, 134, 2353

Shappee B. J., et al., 2014, *ApJ*, 788, 48

Shaw J. S., Caillault J. P., Schmitt J. H. M. M., 1994, in *American Astronomical Society Meeting Abstracts*. p. 85.06

Shi X.-d., Qian S.-b., Li L.-j., Liao W.-p., 2021, *Monthly Notices of the Royal Astronomical Society*, 505, 6166

Skarka M., et al., 2017, *Open European Journal on Variable Stars*, 185, 1

Stepień K., Kiraga M., 2013, *Acta Astron.*, 63, 239

Tokovinin A., Thomas S., Sterzik M., Udry S., 2006, *A&A*, 450, 681

Wilson R. E., 1990, *ApJ*, 356, 613

Wilson R. E., 2012, *The Astronomical Journal*, 144, 73

Wilson R. E., Devinney E. J., 1971, *ApJ*, 166, 605

Wilson R. E., Hamme W. V., 2013, *The Astrophysical Journal*, 780, 151

Worthey G., Lee H. C., 2011, *VizieR Online Data Catalog*, p. J/ApJS/193/1

Wu Y., et al., 2011, *Research in Astronomy and Astrophysics*, 11, 924

Wu Y., Du B., Luo A., Zhao Y., Yuan H., 2014, *Proceedings of the International Astronomical Union*, 10, 340

Xu H.-S., Zhu L.-Y., Thawicharat S., Boonruksar S., 2022, *Research in Astronomy and Astrophysics*, 22, 035024

Zhao G., Zhao Y.-H., Chu Y.-Q., Jing Y.-P., Deng L.-C., 2012, *Research in Astronomy and Astrophysics*, 12, 723

Zhu L., Qian S., 2006, *MNRAS*, 367, 423

Zhu L., Qian S., 2009, in *Murphy S. J., Bessell M. S., eds, Astronomical Society of the Pacific Conference Series Vol. 404, The Eighth Pacific*

Rim Conference on Stellar Astrophysics: A Tribute to Kam-Ching Leung, p. 189

This paper has been typeset from a $\text{\TeX}/\text{\LaTeX}$ file prepared by the author.